Rechargeable iron/air cells employing bifunctional oxygen electrodes of oxide pyrochlores

A. M. Kannan and **A. K. Shukla***
Solid State and Structural Chemistry Unit, Indian Institute of Science, Bangalore-560 012 (India)

(Received November 21, 1990)

Abstract

Prototype secondary iron/air cells comprising pressed-type iron electrodes and oxygen electrodes of some oxide pyrochlores have been assembled and subjected to electrochemical charge/discharge tests for over 150 cycles at various load currents. The cells are found to exhibit little deterioration in performance. Oxygen electrodes using $PbBiRu_2O_{7-y}$ oxide pyrochlores are superior to those with $Pb_2Ir_2O_{7-y}$, except under high-load currents.

Introduction

Among the various types of metal/air batteries under development, the iron/air system is especially attractive as it can utilize iron resources that are virtually inexhaustible. It has a theoretical cell voltage of 1.28 V corresponding to the reaction:

$$2Fe + O_2 + 2H_2O \longrightarrow 2Fe(OH)_2$$

In practice, however, this voltage is never attained owing to mixed potentials arising at both the iron and the air electrodes. The mixed potential at the iron electrode is caused by parasitic hydrogen evolution which results in self discharge [1–3]. The mixed potential at the air electrode is due to peroxide formation [4].

During the last few years, substantial efforts have been made in this laboratory to develop pressed-type iron electrodes as well as some operational bifunctional oxygen electrodes. In this study, these iron electrodes have been integrated with bifunctional oxygen electrodes of $Pb_2Ir_2O_{7-y}$ and $PbBiRu_2O_{7-y}$ oxide pyrochlores to give prototype iron/air cells [5–9]. The performance of the cells under charge/discharge testing is reported in this paper.

Experimental

Active material

The active material for the iron electrodes was obtained by vacuum decomposition of ferrous oxalate. Initially, the oxalate was kept at 200 °C

*Author to whom correspondence should be addressed.

0378-7753/91/$3.50

so as to expel the associated water of hydration. Subsequently, the temperature was raised to 500 °C in order to effect the decomposition of ferrous oxalate [10]. The X-ray diffraction pattern of the decomposed product showed it to be a mixture of α-Fe (15 wt.%) and Fe_3O_4 (85 wt.%). The mean diameter of the particles in this mixture (as measured by a Cilas-Alcatel Granulometer-175) was 13 μm and the BET surface area (as measured by a Micromeritics Rapid Surface Area Analyser-2200) was ~ 12 m^2 g^{-1}.

Pressed-type porous iron electrodes

Pure nickel-based grids (60 mesh cm^{-2}) were subjected to electrochemical degreasing in 20 wt.% NaOH containing 1 vol.% Teepol (a surfactant) at 60 °C under a current of 20 mA cm^{-2} for about 20 min, followed by chemical etching in 1 wt.% $FeCl_3$ for 5 min [5]. With these bare grids, pressed-type iron electrodes having dimensions $5.0 \times 6.5 \times 0.2$ cm^3 were fabricated by hot pressing (112 °C) an appropriate amount of active material that had been mixed for 1800 s with poly(ethylene) (7 wt.%), graphite (10 wt.%) and FeS (1 wt.%). The compaction pressure was 100 kg cm^{-2} and was applied for 180 s [6]. Prior to their use in iron/air cells, the iron electrodes were formed electrochemically as described elsewhere [7]. In brief, the pressed-type iron electrodes were coupled with two excess-capacity sintered nickel electrodes to form secondary nickel/iron cells. The electrolyte was 6 M KOH containing 15 g LiOH per litre of solution. The cell was then charged ($C/10$) for 16 h and discharged ($C/7$) for about 30 cycles at 30 °C until the formation of the iron electrodes was complete.

Fluon-bonded pyrochlore oxide-based bifunctional oxygen electrodes

Oxygen electrodes were prepared as reported previously [8]. In brief, a Fluon-GP2 suspension (16.8 wt.%) was mixed ultrasonically with the required amount of the oxide pyrochlore and dried in an air oven at ~ 100 °C. The dried mass was sandwiched between two degreased nickel wire meshes (2200 mesh cm^{-2}) by cold compaction. The dimensions of these electrodes were similar to those of the iron electrodes.

Charge/discharge tests of iron/air cells

The containers for the prototype iron/air cells were machined from Plexiglas, as this material is not attacked by alkali and is transparent. The rectangular container had side walls with grooves to accommodate the iron electrode in the centre, a lid that held a Luggin capillary for the $Hg/HgO,OH^-$ reference electrode, and, on either side, two oxygen electrode holders with gas inlets. Each oxygen electrode was placed against the cell container using chloroprene rubber gaskets to maintain an airtight assembly; the exposed area of the oxygen electrode was ~ 20 cm^2. The electrolyte was 6 M KOH (without LiOH) and was neither stirred nor circulated. The gas inlet of the cell was connected to a commercial grade oxygen cylinder equipped with a gas-pressure control valve and a mercury manometer.

Charge/discharge tests were conducted on the cells with a d.c. power supply hooked to a Keithley-System-570 Data Acquisition-Workstation in-

terfaced with an IBM-PC/AT. The processor held the current at a constant value and monitored the cell voltage and oxygen electrode potential during both charging and discharging of the cell. The circuit was opened when the cell voltage reached the pre-set cut-off limit. All potentials are reported with regard to the $Hg/HgO,OH^-$ reference electrode. The electrochemical measurements were carried out at room temperature (~ 30 °C).

Results and discussion

Figure 1 shows the capacity behaviour of sulphide-modified iron electrodes in lithiated 6 M KOH solution at 30 °C. The capacity values were calculated from the acquired data up to the first step of discharge, i.e., up to -0.75 V. The depth-of-discharge (DOD) was kept constant by limiting the process to this first step. Although the capacity values varied with cycling, the net charge was kept constant at 150 mA for 16 h. The results in Fig. 1 show that the capacity decreases during the second cycle, and then increased monotonically in subsequent cycles. The stabilized capacity of the electrodes after 30 cycles is ~ 220 mA h g^{-1}. The observed decrease in capacity during the second cycle may be explained as follows. During the first discharge, all the available iron is converted to $Fe(OH)_2$ and a small amount of FeOOH [11, 12]. During the following charge (i.e., the second cycle), however, not all of the mass may transform to active iron, as part of the $Fe(OH)_2$ may become converted to Fe_3O_4 through the reaction:

$$4Fe(OH)_2 \longrightarrow Fe_3O_4 + Fe + 4H_2O.$$

In the following cycles, the depth of penetration of the active material by the electrolyte slowly increases, with the result that more and more iron diffuses to the electrode surface, where it becomes amenable to electrochemical

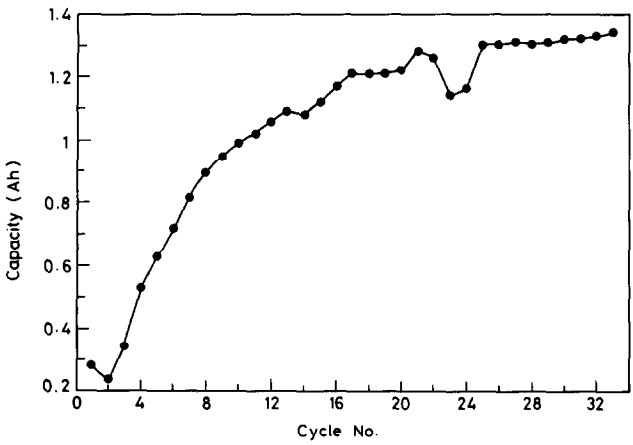

Fig. 1. Capacity during formation cycling for sulphide-modified porous iron electrode (active material = 5 g) in lithiated KOH solution.

reaction, and therefore an increase in capacity is observed. The fluctuations seen in the capacity values are probably due to local changes in pH, temperature, and current distribution inside the electrode pores. Such fluctuations have also been reported by Cnobloch *et al.* [13].

A typical discharge curve for a porous iron electrode in lithiated KOH electrolytes is given in Fig. 2. Step I at about −920 mV corresponds to the oxidation of iron to its divalent state via:

$$Fe + 2OH^- \longrightarrow Fe(OH)_2 + 2e^-.$$

As mentioned above, this study of the performance characteristics of the iron/air cells was restricted to step I. Although the theoretical capacity of iron electrodes to this step is 960 mA h g^{-1}, the observed capacity of the pressed-type iron electrode employed in this study was only 220 mA h g^{-1}. Factors such as passivation/corrosion are responsible for this discrepancy [1, 15]. In step II, which occurs at about −725 mV, the interior active material is utilized and, probably, iron is oxidized to its divalent and/or trivalent states. A third step is also observed at about −660 mV; this is similar to that reported by Geronov *et al.* [14] for iron electrodes in lithiated KOH electrolyte.

In order to study the performance characteristics of an iron/air cell employing a $Pb_2Ir_2O_{7-y}$ pyrochlore-based, bifunctional oxygen electrode, the cell was discharged at various load currents (between 50 and 200 mA) and recharged at load currents of 100 and 150 mA. The discharge characteristics are given in Fig. 3. Little variation in the cell capacity was observed with increase in load current. The cell capacity as a function of cycle life is presented in Fig. 4. The data reveal that the cell displayed higher capacity values during the discharge cycles following a deep discharge. This observation is in agreement with that reported elsewhere for Ni/Fe cells [16]. A typical deep-discharge curve of the iron/air cell is shown in Fig. 5. Unlike the

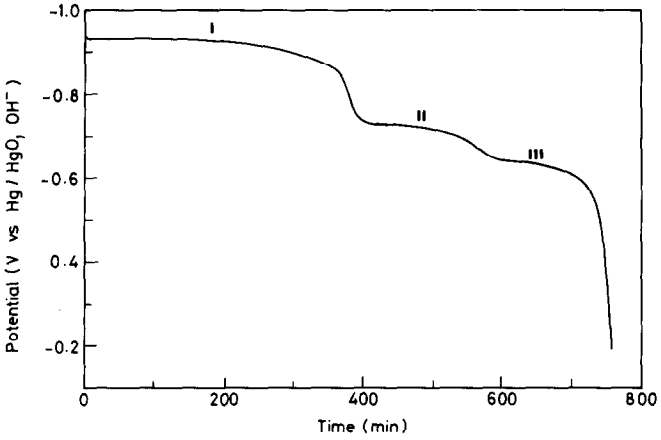

Fig. 2. Typical discharge curve for sulphide-modified porous iron electrode (active material = 5 g, discharge current = 200 mA) in lithiated KOH solution at 30 °C.

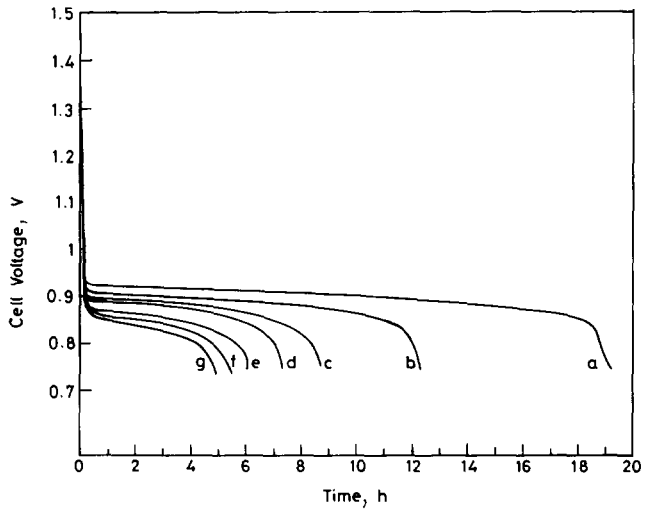

Fig. 3. Discharge characteristics of iron/air secondary cell ($Pb_2Ir_2O_{7-y}$ oxygen electrode and 6 M KOH) at 30 °C and load current: (a) 50; (b) 75; (c) 100; (d) 125; (e) 150; (f) 175; (g) 200 mA.

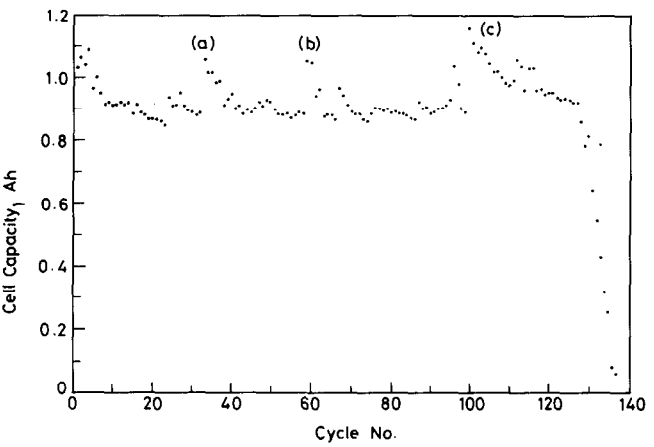

Fig. 4. Capacity of iron/air secondary cell ($Pb_2Ir_2O_{7-y}$ oxygen electrode and 6 M KOH) at 30 °C. (a), (b) and (c) are capacities following a deep discharge.

behaviour of iron in lithiated KOH electrolyte (Fig. 2), electrodes in unlithiated KOH electrolyte were found to exhibit only two steps during deep discharge of the cell.

Figure 6 illustrates the long-term performance of a $Pb_2Ir_2O_{7-y}$-based oxygen electrode with an exposed area of 20 cm^2 in an iron/air cell both during charge and discharge at various load currents. It can be seen that the electrode potentials for the oxygen reduction and evolution reactions were quite stable during the charge/discharge tests. The oxygen evolution potential during charging was as low as 500 mV at 150 mA. Gibney and

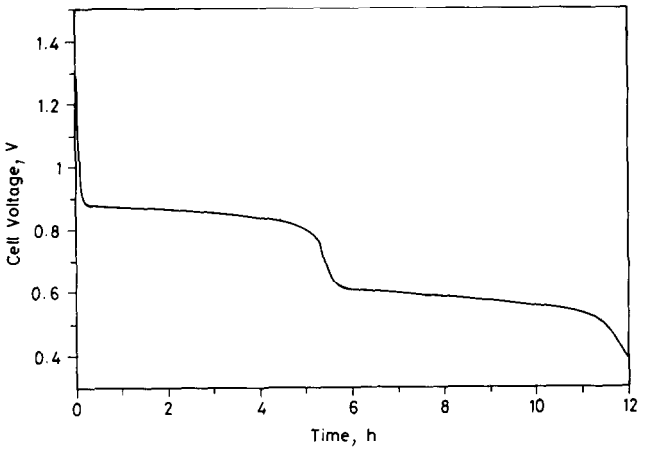

Fig. 5. Typical deep-discharge curve for iron/air cell ($Pb_2Ir_2O_{7-y}$ oxygen electrode and 6 M KOH) at 30 °C and a load current of 150 mA.

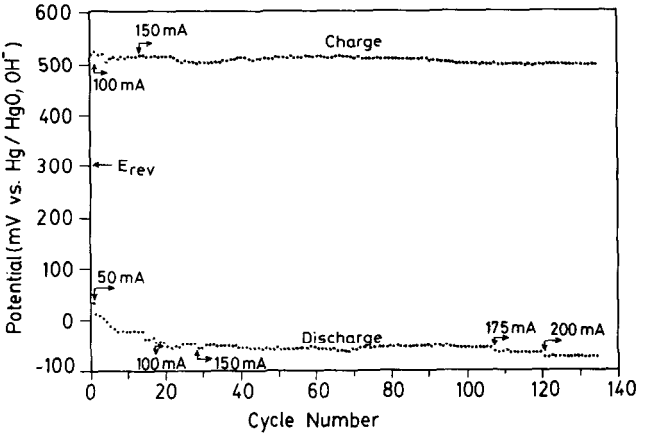

Fig. 6. Performance of $Pb_2Ir_2O_{7-y}$-based oxygen electrode (active area: 20 cm^2) during charge/discharge cycling of secondary iron/air cell (6 M KOH) under various load currents at 30 °C.

Zuckerbrod [17] have reported similar values. Although there was no noticeable change in oxygen electrode performance during either charging or discharging of the cell (Fig. 6), a decrease in the overall cell capacity was noticed. This was found to be due to the loss in capacity of iron electrodes; the capacity could be retrieved by adding 1.5 wt.% LiOH to the electrolyte.

Figure 7 shows the discharge characteristics at three different load currents of an iron/air cell employing a $PbBiRu_2O_{7-y}$ pyrochlore oxide-based, bifunctional oxygen electrode. Clearly, there is no change in the cell capacity. The corresponding performance of the oxygen electrode is summarized in Fig. 8. It is concluded that this electrode is superior to the $Pb_2Ir_2O_{7-y}$

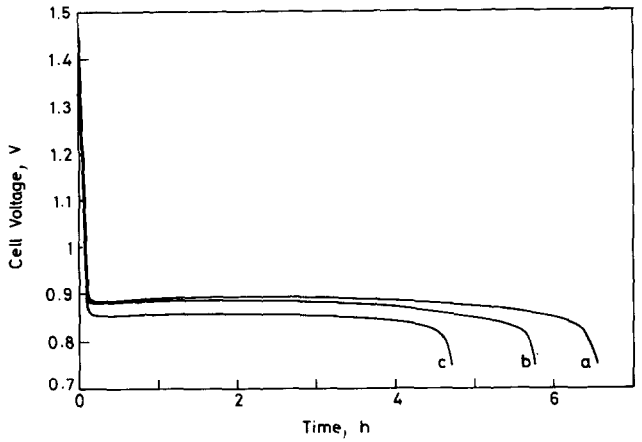

Fig. 7. Discharge characteristics of iron/air secondary cell ($PbBiRu_2O_{7-y}$ oxygen electrode and 6 M KOH) at 30 °C and load current: (a) 150; (b) 175; (c) 200 mA.

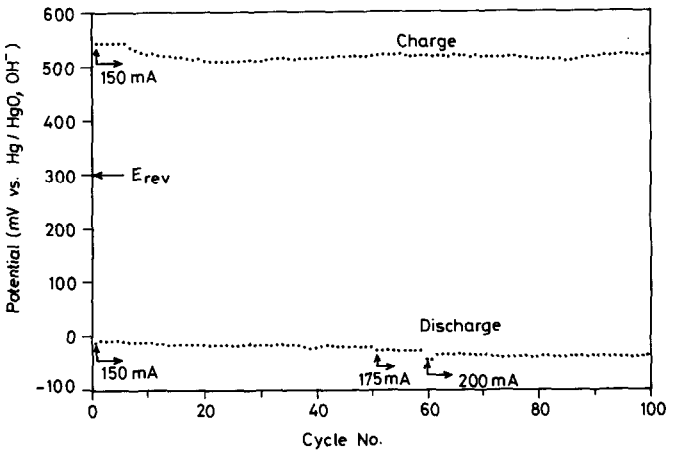

Fig. 8. Performance of $PbBiRu_2O_{7-y}$-based oxygen electrode (active area: 20 cm^2) during charge/discharge cycling of secondary iron/air cell (6 M KOH) under various load currents at 30 °C.

bifunctional oxygen electrode, except at high load currents. The cell capacity as a function of cycle life is given in Fig. 9. The data show a fall in capacity after 85 cycles. This was caused by a loss in capacity of the iron electrode and, as before, the phenomenon could be reversed by adding 1.5 wt.% LiOH to the electrolyte. It has been claimed [18, 19] that LiOH increases the charge acceptance of the iron electrode by suppressing H_2 evolution. Typical data for the variation in oxygen electrode potential during charge/discharge tests conducted on prototype cells are presented in Fig. 10. It is clear that the oxygen electrode potential remains virtually invariant.

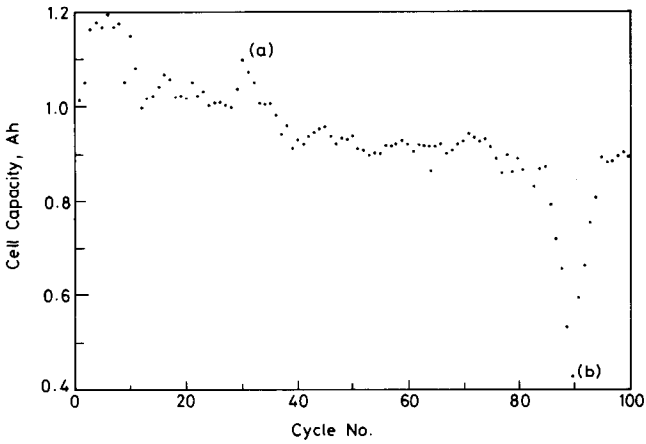

Fig. 9. Capacity of iron/air secondary cell ($PbBiRu_2O_{7-y}$ bifunctional oxygen electrode and 6 M KOH) at 30 °C. (a) represents the capacity value following a deep discharge.

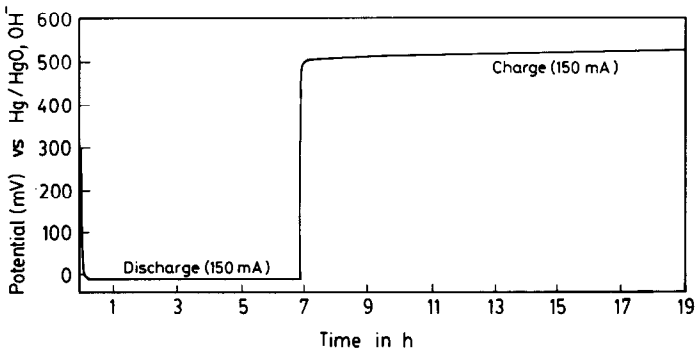

Fig. 10. Potential of $PbBiRu_2O_{7-y}$ bifunctional oxygen electrode (active area: 20 cm^2) during discharge/charge of secondary iron/air cell.

Acknowledgements

The authors are indebted to Professor S. Sathyanarayana for advice and encouraging support throughout this work, and to Dr K. Vijayamohanan for helpful discussions. The authors are grateful to the Department of Non-Conventional Energy Sources, Government of India, New Delhi, for financial assistance. One of us (AMK) thanks the Council of Scientific and Industrial Research, New Delhi, for the award of a Senior Research Fellowship.

References

1 S. Hills and A. J. Salkind, *Proc. 22nd Power Sources Symp.*, PSC Committee, NJ, 1968, p. 66.
2 L. Ojefors, *J. Electrochem. Soc.*, *123* (1976) 1139.

3 H. N. Sieger, *Proc. 16th Intersoc. Energy Conv. Eng. Conf., Atlanta, GA, Aug. 9–14, 1982*, pp. 102–110.
4 E. Yeager, in U. Landau, E. Yeager and D. Kortan (eds.), *Electrochemistry in Industry: New Directions*, Plenum, New York, 1982, p. 29, and refs. therein.
5 K. Vijayamohanan, *Ph.D. Thesis*, Indian Institute of Science, Bangalore, 1989.
6 K. Vijayamohanan, A. K. Shukla and S. Sathyanarayana, *Indian J. Technol., 24* (1986) 436.
7 K. Vijayamohanan, A. K. Shukla and S. Sathyanarayana, *J. Power Sources, 32* (1990) 329.
8 A. M. Kannan, A. K. Shukla and S. Sathyanarayana, *J. Electroanal. Chem., 281* (1990) 339.
9 K. Vijayamohanan, A. K. Shukla and S. Sathyanarayana, *Electrochim. Acta, 36* (1991) 369.
10 D. Dollimore and Griffiths, *J. Thermal Anal., 2* (1970) 240.
11 H. G. Silver and E. Lekas, *J. Electrochem. Soc., 117* (1970) 5.
12 V. M. Fantgoff and L. M. Lishanskii, *Elektrokhimiya, 18* (1982) 647.
13 H. Cnobloch, D. Groppel, D. Kuhl, W. Nippe and G. Siemsen, in D. H. Collins (ed.), *Power Sources 5*, Academic Press, London, 1975, p. 261.
14 Y. Geronov, T. Tomov and S. Georgiev, *J. Appl. Electrochem., 5* (1975) 351.
15 S. U. Falk and A. J. Salkind, *Alkaline Storage Batteries*, Wiley, New York, 1969, p. 79.
16 M. Cenek, J. Kazelle and B. Wilczek, *Proc. Int. Symp. Mechanization and Automation in Chemical Power Sources Production, Poznan, Poland, Oct. 11–13, 1988*, pp. 27, 221–240.
17 A. Gibney and D. Zuckerbrod, in J. Thomson (ed.), *J. Power Sources 9*, Academic Press, London, 1982, p. 143.
18 M. Hara, *Jpn. Kokai Tokkyo Koho JP 6 319 771*, 27 Jan. 1988, Applic. 11 July 1986, 6 pp.
19 N. A. Hampson, R. J. Latham, A. N. Oliver, R. V. Giles and P. C. Tones, *J. Appl. Electrochem., 3* (1973) 61.